Numerical simulation of quasi-brittle fracture using damaging cohesive surfaces

Tijssens, M.G.A.; Sluys, B.L.J.; van der Giessen, E.

Published in:
European Journal of Mechanics A-Solids

DOI:
10.1016/S0997-7538(00)00190-X

Publication date:
2000

Eur. J. Mech. A/Solids 19 (2000) 761–779

S0997-7538(00)00190-X/FLA

Numerical simulation of quasi-brittle fracture using damaging cohesive surfaces

Martin G.A. Tijssens *, Bert L.J. Sluys, Erik van der Giessen

Delft University of Technology, Koiter Institute Delft, Stevinweg 1, 2628 CN, Delft, The Netherlands

(Received 28 January 2000; revised and accepted 1 March 2000)

Abstract – The cohesive surface methodology is used in a numerical study of fracture of concrete. The traction vs. separation response is governed by an isotropic damage law in which damage evolves according to a prescribed one-dimensional linear or exponential softening law. Cohesive surfaces are immersed in the continuum to allow for a maximum freedom of crack path selection. The single edge notched four point shear beam and the double edge notched tensile bar are used to study: (i) the influence of the tangential cohesive response on the development of the fracture path and (ii) the mesh alignment sensitivity. It is shown that in the present formulation, the tangential cohesive response has a minor influence on both crack path and global characteristics. Mesh alignment does have a significant influence on the outcome of the numerical analysis. © 2000 Éditions scientifiques et médicales Elsevier SAS

cohesive surface / isotropic damage / concrete / finite elements

1. Introduction

Concrete is a highly heterogeneous material, not only due to the presence of aggregates but also due to the microstructure of cement paste, which contains hydrated grains, microcracks and voids. Fracture processes in concrete have been observed to be a continuous process of creating and linking up of microcracks. Due to the mutual avoidance of microcracks, bridges between cracks form. After an initial steep softening response these bridges result in a long tail in the load-displacement curve (Van Mier, 1997).

Many attempts have been made to develop micromechanical models for brittle fracture in heterogeneous materials. Koiter (1959) presented an analytical solution to the problem of an infinite array of collinear cracks loaded by a remote traction perpendicular to the plane of the cracks. Westmann (1965) presented the analytical solution to the problem of a penny-shaped crack loaded by shear tractions. Ortiz (1988) used the results of Koiter (1959) to develop a cohesive surface model for brittle solids valid for normal crack face loading only. Closed-form solutions to the problem of a penny-shaped crack loaded by arbitrary tractions were given by Fabrikant (1990). These expressions were used by Huang and Karihaloo (1992) to study the tension softening response of brittle solids. Kachanov and Laures (1989) used the results of Fabrikant (1990) to study the effect of microcrack interaction on the stress intensity factors. These studies on idealized microstructures have contributed much to understanding the fracture behavior of quasi-brittle materials. However, to obtain constitutive models for the fracture behaviour of concrete still much more research is needed.

Motivated by the random character of fracture processes in concrete, strength and stiffness degradation and fracture of concrete has been described by continuum damage modelling for a long time (Kachanov, 1986). In addition to isotropic damage models, anisotropic damage models have been proposed (Govindjee et al., 1995;

* Correspondence to: M.G.A. Tijssens, Stevinweg 1, 2628 CN, Delft, The Netherlands. E-mail: M.G.A.Tijssens@wbmt.tudelft.nl, tel: (+31) 15 278 6602, fax: (+31) 15 278 6383.

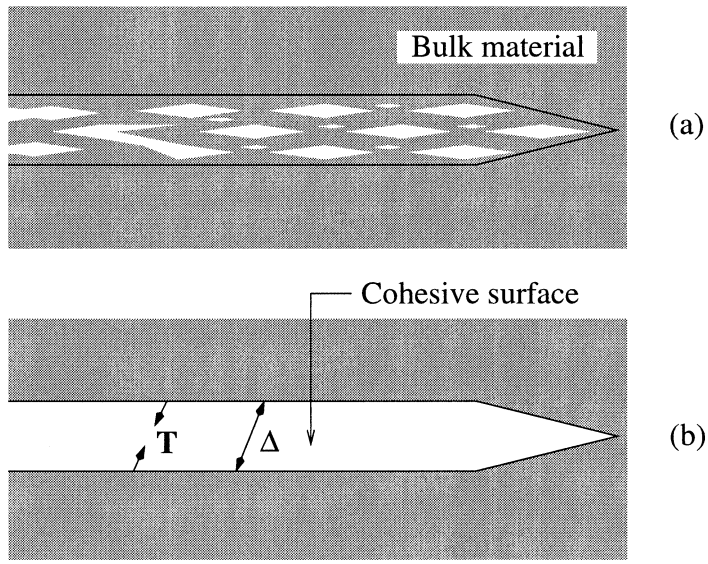

Figure 1. Illustration of capturing a microcracked zone into a cohesive surface.

Meschke et al., 1998; Fichant et al., 1999) to better capture the stiffness degradation of concrete during damage evolution. Non-local (Bažant et al., 1984; Pijaudier-Cabot and Bažant, 1987; Bažant and Pijaudier-Cabot, 1988) and gradient damage models (Peerlings et al., 1996) have been proposed to remedy the loss of ellipticity of the equilibrium equations and resulting mesh sensitivity problems. Besides the continuum damage modelling of fracture, discrete crack or cohesive surface models of various sophistication (e.g. Carol et al., 1997; Lourenço and Rots, 1997) have been proposed.

The model presented in this paper is based on a local, isotropic damage formulation for the constitutive response of a cohesive surface. A cohesive surface relates the traction $\boldsymbol{T}$, transmitted over the surface, to the separation $\boldsymbol{\Delta}$ between the surfaces, see *figure 1*. In contrast to the continuum damage models in which damage affects the stiffness of a material volume, damage evolution in the cohesive surface model affects the ability to transmit tractions over the cohesive surface. While the bulk of the material remains elastic, the model thus captures anisotropic damage evolution in a natural way since damage develops only on specific planes. Fracture of the material now progresses solely based on the strength degradation in the cohesive surfaces and the interaction with the intact, elastic, regions of the material.

In section 2 we will present the cohesive traction–separation relation, after which the numerical implementation is given in section 3. In sections 4 and 5 we use the single edge notched shear beam and the double edge notched tensile bar, respectively, to study concrete fracture and mesh alignment sensitivity of the cohesive surface methodology. Concluding remarks are given in section 6.

2. Damage modelling in cohesive surfaces

The traditional isotropic damage relation between the traction vector and the separation vector of a cohesive surface reads

$$\boldsymbol{T} = (1 - \omega)\boldsymbol{D}\boldsymbol{\Delta}, \tag{1}$$

in which $\boldsymbol{T} = [T_n\ T_t]^T$ and $\boldsymbol{\Delta} = [\Delta_n\ \Delta_t]^T$ contain the normal and tangential components of the traction and separation to the cohesive surface, respectively. For the material matrix $\boldsymbol{D}$ we assume that there is no coupling between normal and tangential separation as long as damage has not initiated and that the normal and tangential stiffnesses are equal, i.e.,

$$\boldsymbol{D} = d_0 \boldsymbol{I}, \tag{2}$$

where $\boldsymbol{I}$ is the identity matrix and d_0 is the elastic cohesive surface stiffness.

The damage variable ω describes the state of damage and varies between 0 and 1. Ideally, a micromechanically based evolution of the damage variable ω should be used, but such relations are not available. We therefore use a phenomenological evolution law and concentrate on the general aspects that a cohesive traction law must fulfill in order to realistically describe concrete fracture.

In continuum damage models, one generally assumes the damage variable ω to be a function of a history parameter κ, which is a function of some measure of equivalent strain ε^{eq}. Various definitions of the equivalent strain ε^{eq} have been proposed (see, e.g., Peerlings et al., 1998) of which we mention the definition given by Mazars (see, e.g., Mazars and Pijaudier-Cabot, 1989), in which only the positive, principle strains are used

$$\varepsilon_{eq} = \sqrt{\sum_{i=1}^{3} \langle \varepsilon_i \rangle^2}, \tag{3}$$

where $\langle\,\rangle$ denote the Macaulay brackets.

Motivated by the relative simplicity of Mazars' criterion and following Camacho and Ortiz (1996) we let ω be a function of the equivalent one-dimensional cohesive separation ζ defined by

$$\zeta^2 = \Delta_n^2 + \alpha \Delta_t^2 \tag{4}$$

in which the influence of the tangential separation Δ_t can be varied through the parameter α. The rate equations for the cohesive surface are now obtained as

$$\dot{\boldsymbol{T}} = (1-\omega)\boldsymbol{D}\dot{\boldsymbol{\Delta}} - \dot{\omega}\boldsymbol{D}\boldsymbol{\Delta} \tag{5}$$

in which $\dot{\omega}$ is obtained through

$$\dot{\omega} = \frac{\mathrm{d}\omega}{\mathrm{d}\zeta}\left[\frac{\partial \zeta}{\partial \Delta_n}\dot{\Delta}_n + \frac{\partial \zeta}{\partial \Delta_t}\dot{\Delta}_t\right]. \tag{6}$$

Substitution of (6) into (5) results in the rate constitutive equations for the cohesive surfaces

$$\begin{pmatrix} \dot{T}_n \\ \dot{T}_t \end{pmatrix} = \begin{pmatrix} (1-\omega)d_0 - \dfrac{\mathrm{d}\omega}{\mathrm{d}\zeta}\dfrac{\partial \zeta}{\partial \Delta_n} d_0 \Delta_n & -\dfrac{\mathrm{d}\omega}{\mathrm{d}\zeta}\dfrac{\partial \zeta}{\partial \Delta_t} d_0 \Delta_n \\ -\dfrac{\mathrm{d}\omega}{\mathrm{d}\zeta}\dfrac{\partial \zeta}{\partial \Delta_n} d_0 \Delta_t & (1-\omega)d_0 - \dfrac{\mathrm{d}\omega}{\mathrm{d}\zeta}\dfrac{\partial \zeta}{\partial \Delta_t} d_0 \Delta_t \end{pmatrix} \begin{pmatrix} \dot{\Delta}_n \\ \dot{\Delta}_t \end{pmatrix}. \tag{7}$$

The term $\mathrm{d}\omega/\mathrm{d}\zeta$ is defined through the one-dimensional relation

$$\sigma(\zeta) = \big(1 - \omega(\zeta)\big) d_0 \zeta \tag{8}$$

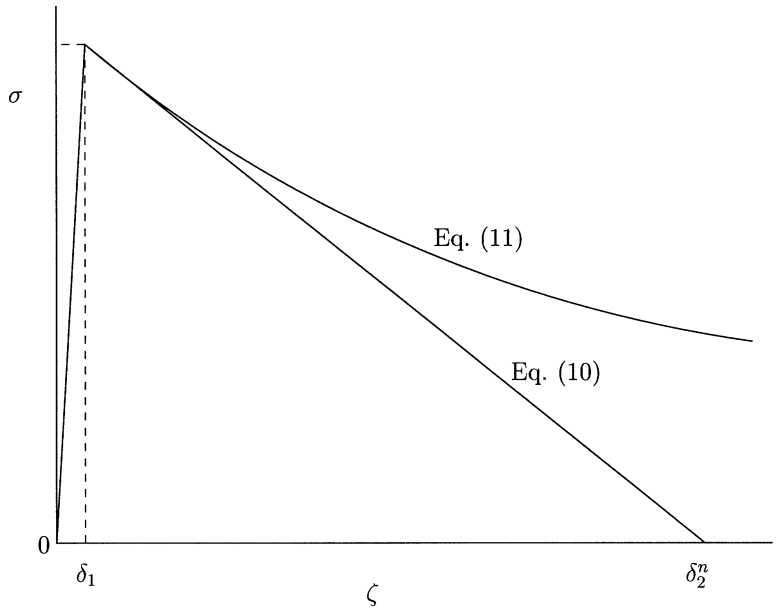

Figure 2. Illustration of the one-dimensional softening responses given in (10) and (11) with $\beta = \delta_1/(\delta_2^n - \delta_1)$.

in which σ and ζ are the one-dimensional traction and separation of the cohesive surface. Hence

$$\frac{\mathrm{d}\omega}{\mathrm{d}\zeta} = \frac{1}{d_0\zeta}\left[\frac{\sigma(\zeta)}{\zeta} - \frac{\mathrm{d}\sigma(\zeta)}{\mathrm{d}\zeta}\right]. \tag{9}$$

In this paper we limit ourselves to damage initiation and growth under tensile stresses. Initially, the cohesive surface constitutive response is assumed to be elastic according to $\sigma(\zeta) = d_0\zeta$ where we take $d_0 = \sigma_{\max}/\delta_1$ with $\sigma_{\max}$ the maximum tensile strength of the cohesive surface and δ_1 the value of the equivalent cohesive separation ζ for which damage initiates. For $\zeta > \delta_1$ we assume a softening response. Common approaches to define the softening response after peak load are to define linear or exponential softening. These will be adopted in this paper according to

$$\sigma(\zeta) = \sigma_{\max}\frac{\delta_2^n - \zeta}{\delta_2^n - \delta_1}, \quad \zeta \geqslant \delta_1, \tag{10}$$

for linear softening and

$$\sigma(\zeta) = \sigma_{\max}\exp\left[\beta\left(1 - \frac{\zeta}{\delta_1}\right)\right], \quad \zeta \geqslant \delta_1, \tag{11}$$

for exponential softening. The rate of softening is determined by δ_2^n. The localization of deformation and thus the prediction of the final fracture path is to a large extent determined by the initial softening of the cohesive law. For this reason, the value of β in the exponential softening is taken as $\delta_1/(\delta_2^n - \delta_1)$ which results in equal initial softening behaviour for linear and exponential softening. The softening response is illustrated in *figure 2*.

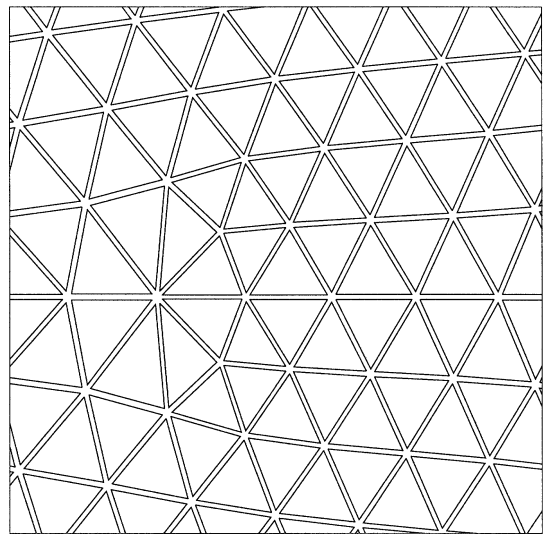

Figure 3. Representative part of a finite element mesh with embedded cohesive surfaces. The continuum elements have been shrunk for illustration purposes.

3. Numerical implementation

Confining attention here to brittle fracture in an elastic material, we do not expect large strains in the bulk. However, finite strain effects may be of importance in the neighbourhood of the crack tip. Therefore we do account for finite strains in the continuum description, using a Total Lagrangian description for which the incremental equilibrium equations are specified through the rate form of the principle of virtual work:

$$\Delta t \int_V (\dot{\tau}^{ij}\delta\eta_{ij} + \tau^{ik}\dot{u}^j_{,k}\delta u_{j,i})\,\mathrm{d}V + \Delta t \int_{S_i} \dot{T}_\alpha \delta\Delta_\alpha \,\mathrm{d}S$$
$$= \Delta t \int_{S_u} \dot{t}^i \delta u_i \,\mathrm{d}S - \left[\int_V \tau^{ij}\delta\eta_{ij}\,\mathrm{d}V + \int_{S_i} T_\alpha \delta\Delta_\alpha \,\mathrm{d}S - \int_{S_u} t^i \delta u_i \,\mathrm{d}S\right] \tag{12}$$

in which Δt is the time increment, V and S_u are the volume and outer surface of the body in the reference configuration and S_i is the current internal cohesive surface. The latter is the collection of all cohesive surface elements contained in V. Elasticity of the bulk is incorporated through the well-known hypoelastic relation in terms of the second Piola–Kirchhoff stress $\boldsymbol{\tau} = \tau^{ij}\boldsymbol{e}_i\boldsymbol{e}_j$ and the Lagrangian strain $\boldsymbol{\eta} = \eta_{ij}\boldsymbol{e}^i\boldsymbol{e}^j$:

$$\dot{\tau}^{ij} = \mathcal{L}^{ijkl}\dot{\eta}_{kl} \tag{13}$$

in which $\mathcal{L}^{ijkl}$ is the material modulus tensor, which for an isotropic elastic material is expressed in terms of Young's modulus E and Poisson's ratio ν.

The term in (12) between square brackets is the equilibrium correction which is zero for a state of perfect equilibrium. This term is included to prevent drifting of the solution from the true equilibrium path due to the finite time increments. The finite element equations are obtained by eliminating the stress rates $\dot{\tau}^{ij}$ using (13) and eliminating the cohesive surface traction rates using (7) and (9).

In the discretization of the total cohesive surface area S_i, cohesive surface elements are used over the entire volume, as pioneered in (Xu and Needleman, 1994) and shown in *figure 3*. This way, crack initiation and

propagation are independent of criteria other than the description of the failure processes in the cohesive surfaces.

In this paper the cohesive surface damage model will be applied to fracture of a single edge notched (SEN) four point shear beam and a double edge notched (DEN) tensile bar. Indirect displacement control (see de Borst, 1987) is used to control the load increments. The procedure is as follows: the set of incremental equilibrium equations can be written as

$$\begin{bmatrix} \boldsymbol{K}_{ff} & \boldsymbol{K}_{fp} \\ \boldsymbol{K}_{pf} & \boldsymbol{K}_{pp} \end{bmatrix} \begin{bmatrix} \Delta \boldsymbol{U}_f \\ \Delta \boldsymbol{U}_p \end{bmatrix} = \begin{bmatrix} \Delta \boldsymbol{F}_f \\ 0 \end{bmatrix} + \begin{bmatrix} \boldsymbol{R}_f \\ \boldsymbol{R}_p \end{bmatrix} \tag{14}$$

in which $\Delta \boldsymbol{U}_f$ and $\Delta \boldsymbol{U}_p$ are the free and prescribed degrees of freedom respectively; $\Delta \boldsymbol{F}_f$ is the incremental external force vector, and $\boldsymbol{R}_f$ and $\boldsymbol{R}_p$ contain the equilibrium correction and reaction forces respectively. Using a load factor $\Delta\lambda$ to define

$$\Delta \boldsymbol{F}_f = \Delta\lambda \hat{\boldsymbol{F}}_f, \qquad \Delta \boldsymbol{U}_p = \Delta\lambda \hat{\boldsymbol{U}}_p \tag{15}$$

the solution of the incremental set of equilibrium equations is obtained as

$$\Delta \boldsymbol{U}_f = \Delta\lambda \boldsymbol{K}_{ff}^{-1} \{ \hat{\boldsymbol{F}}_f - \boldsymbol{K}_{fp} \hat{\boldsymbol{U}}_p \} + \boldsymbol{K}_{ff}^{-1} \boldsymbol{R}_f. \tag{16}$$

The load factor $\Delta\lambda$ is chosen such that a constraint equation is fulfilled. The constraint equations used in the applications will be given in sections 4 and 5.

4. Application 1: Fracture of a SEN beam

4.1. Problem formulation

The SEN beam has become a standard geometry on which computational models for concrete fracture are tested. Specifically, the SEN beam has been extensively used to determine whether concrete fails due to tensile stresses only or by a combination of tensile and shearing stresses. Here we follow the SEN beam geometry as used by Schlangen (1993) and analysed numerically by Peerlings et al. (1998), depicted in *figure 4*. The boundary conditions are specified by locking the upper right corner of the beam and by preventing the lower right corner from displacing in the horizontal direction. The load is applied through a concentrated vertical force of $1/11P$ on the lower left corner of the beam and a constant pressure on the middle supports with a resultant vertical force of $10/11P$. The support width is 20 mm with the centre displaced 20 mm out of the centre line of the beam. The constraint equation that is used to solve (16) is based on the Crack Mouth Sliding Displacement (CMSD), i.e. $u_y^b - u_y^a$ in *figure 4*.

A typical finite element mesh of the SEN beam is shown in *figure 5*. The use of cohesive surfaces is limited to the middle part of the beam since no fracture is expected to occur near the outer regions. Within the section, where cohesive surfaces are used, all continuum elements are surrounded by cohesive surfaces. No assumption on the fracture path is made a priori and the description of the evolution of damage in the cohesive surfaces together with the elastic description of the continuum determines where the beam will fail.

To compare the numerical results with experiments, we use the experimental results of Schlangen (1993) for normal concrete with maximum aggregate diameter of 8 mm. The tensile strength of this type of concrete is given as 3.44 MPa. In the numerical calculations, the tensile strength of the cohesive surfaces is set to $\sigma_{\max} = 3$ MPa, Young's modulus $E = 20\,000$ MPa and Poisson's ratio $\nu = 0.3$. The threshold value δ_1 of the equivalent separation ζ is given a small value such that the elastic deformation of the cohesive surfaces is

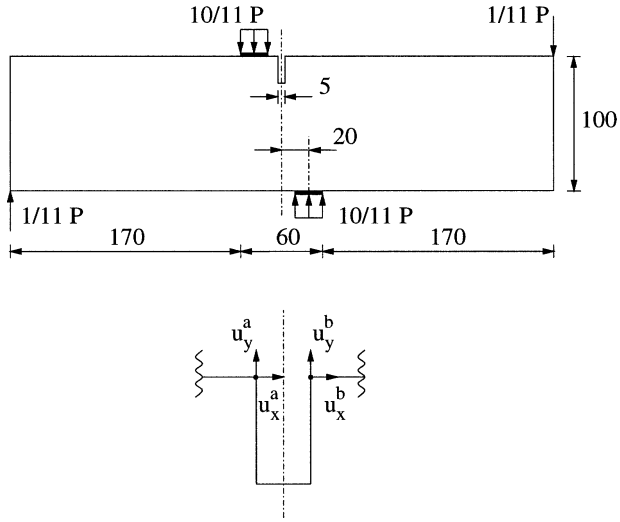

Figure 4. Configuration of the SEN beam. All lengths are in mm.

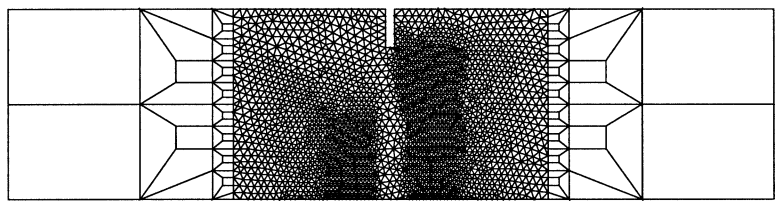

Figure 5. Finite element mesh of the SEN beam.

negligible compared to the elastic deformation of the continuum. For simplicity we assume the parameters δ_2^n and δ_2^t to be equal. Their value is determined as follows.

The fracture energy G_f of normal concrete is given approximately as $G_f = 0.08$ N/mm (see, e.g., Van Mier, 1997). Using local exponential softening as an example, see (11), the fracture energy is $G_f = \sigma_{\max}\delta_1/\beta$. Assuming the elastic contribution to the fracture energy to be small, i.e. $(\delta_1 \to 0)$, and using the definition of β given in section 2 this reduces to $G_f = \sigma_{\max}\delta_2^n$. For the values of G_f and $\sigma_{\max}$ of normal concrete as given previously, this then results in $\delta_2^n = 0.023$ mm. In our calculations we have used $\delta_2^n = 0.02$ mm. This is of the same order of magnitude as used by Hillerborg et al. (1976).

4.2. The influence of local softening characteristics

The softening characteristics of concrete on a local scale are still unknown. Crack growth in concrete, as well as in many other brittle heterogeneous materials, has often been described as a result of the growth of microcracks. Ortiz (1988) developed an effective traction–separation law for a cohesive zone based on the growth and interaction of plane strain microcracks. Huang and Karihaloo (1992) developed an effective traction–separation law for a doubly infinite array of penny-shaped microcracks. These studies indicate that the traction–separation relation for a cohesive surface based on growth of microcracks is more closely related to exponential softening than linear softening. The physical explanation is that local softening behaviour, as governed by the growth of microcracks, starts out with a strong softening due to the sudden development and growth of many microcracks. This process comes to a stop later on due to the mutual avoidance of

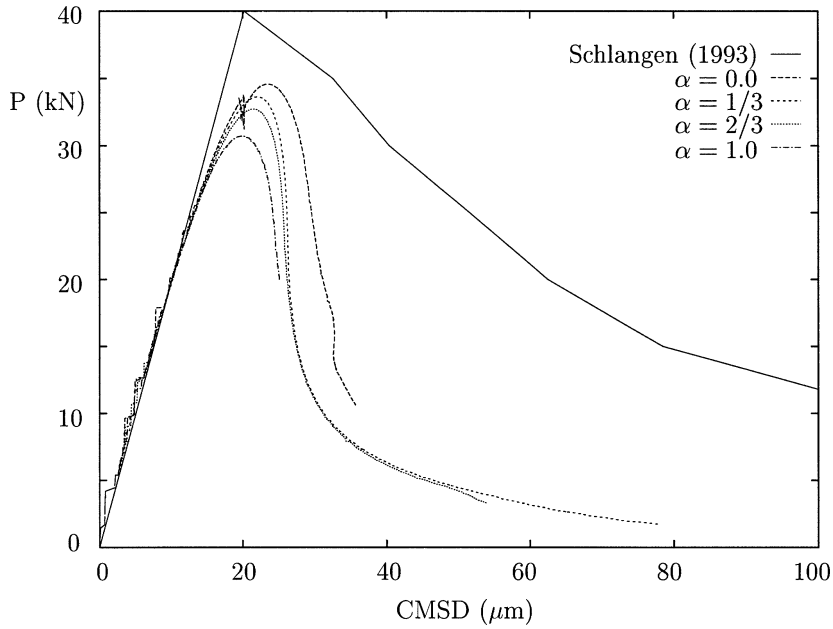

Figure 6. Development of the global load with crack mouth sliding displacement (CMSD) for the local linear softening damage model, in comparison with experimental results of Schlangen (1993).

microcracks, which leads to the formation of many crack bridges (Van Mier, 1997). This stage and the growth of microcracks to larger dimensions is accompanied by a more gradual reduction in cohesive traction with increasing separation.

Within our simple cohesive surface model based on damage, linear and exponential softening have been used to analyse the global load vs. crack mouth sliding displacement relation as well as the local crack pattern. The influence of the tangential sliding displacement of the cohesive surfaces is governed by the value of α in (4) which is taken to have values 0, $1/3$, $2/3$ or 1. The discretization is constant for all cases considered here.

Considering the global load vs. CMSD curves for linear softening in *figure 6*, it is clear that the linear softening behaviour in the cohesive surfaces results in a global post-peak behaviour that is too brittle. Exponential softening (*figure 7*) performs somewhat better, but even here we see a too brittle softening behaviour. The parameter α in (4) has been adjusted in the calculations to include the possibility of damage growth due to tangential separation of the cohesive surface. For $\alpha = 0$ there is no influence of tangential separation in either damage initiation or growth, whereas for $\alpha = 1$ both normal and tangential separation have an equal influence on the damage development. From the global load vs. CMSD curves given in *figure 6* and *7* it can be observed that the influence of the tangential sliding displacement does not dominate the global response of the SEN beam. Also the final fracture paths for exponential softening shown in *figure 9*, which are all virtually identical, seem to agree with this conclusion. However, we do observe a change in failure mode for linear softening as seen in *figure 8a* as compared to *figures 8b–d*. When some influence of tangential separation is included, thereby reducing the normal separation needed to reach the damage initiation criterion (see (4)), a new crack in the middle of the beam does not become dominant (as in *figure 8a*) and a straight crack runs from the notch toward the lower right support (*figures 8b–d*). Since the local linear softening results in a too brittle global post-peak behaviour for all values of α, we must conclude that the failure mode depicted in *figure 8a* is not likely to represent a physical fracture mode of the concrete SEN beam.

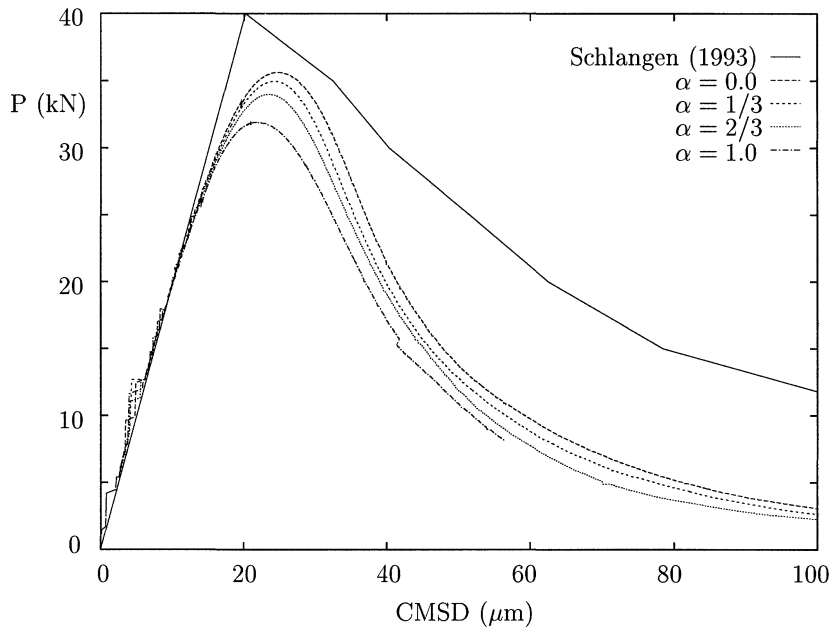

Figure 7. Development of the global load with crack mouth sliding displacement (CMSD) for the local exponential softening damage model, in comparison with experimental results of Schlangen (1993).

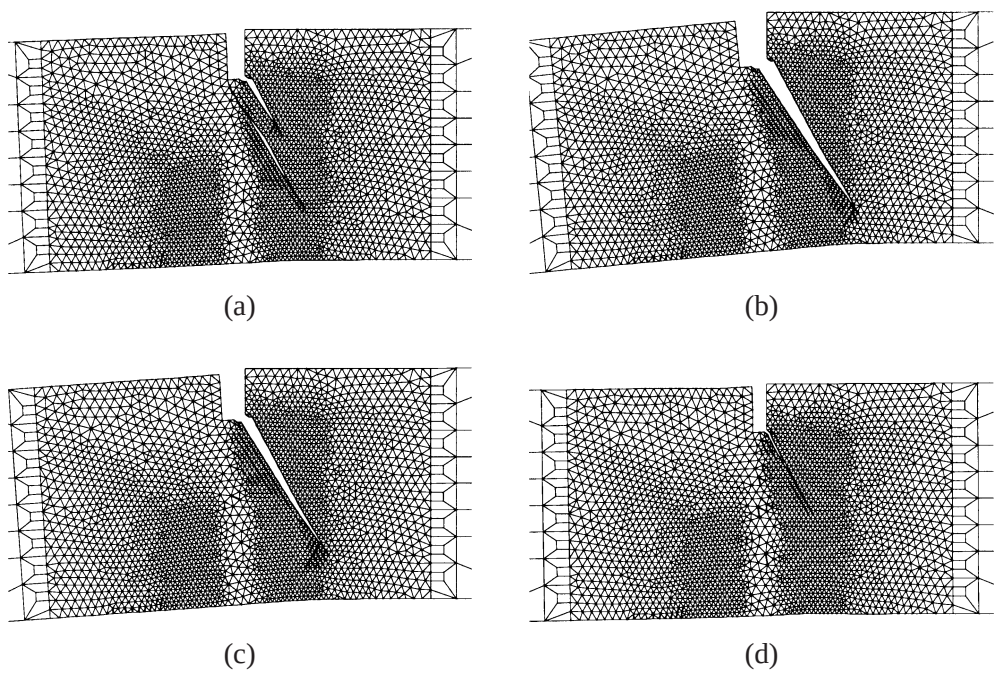

Figure 8. Final deformation of the SEN beam using linear softening and (a) $\alpha = 0$, (b) $\alpha = 1/3$, (c) $\alpha = 2/3$, (d) $\alpha = 1$. Displacements have been magnified by a factor of 50.

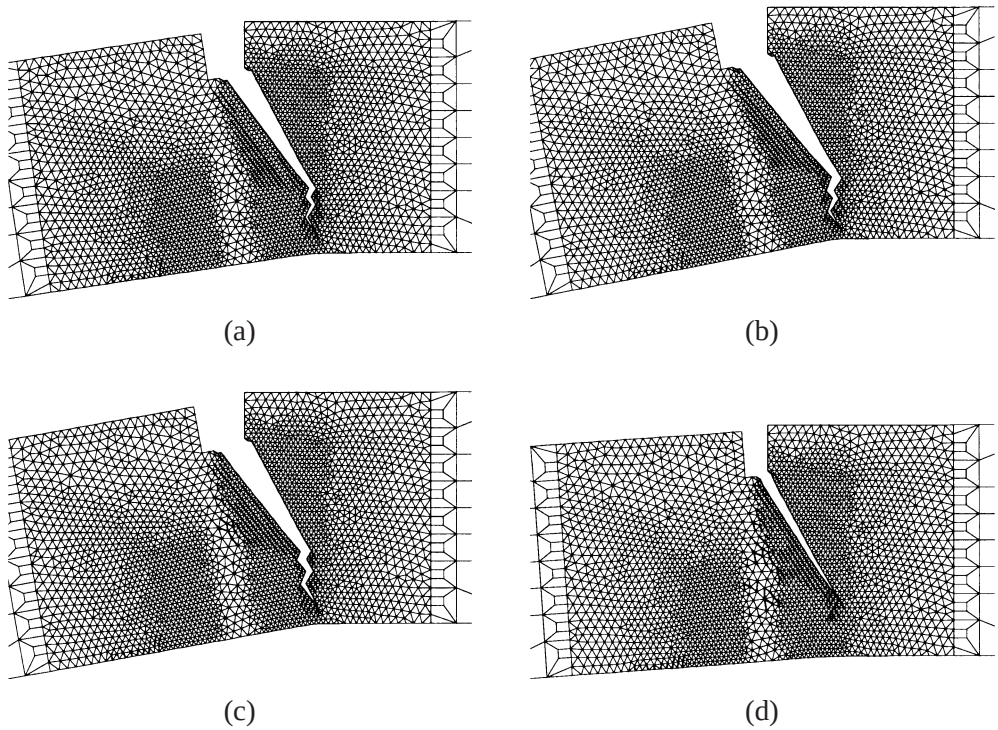

Figure 9. Final deformation of the SEN beam using exponential softening and (a) $\alpha = 0$, (b) $\alpha = 1/3$, (c) $\alpha = 2/3$, (d) $\alpha = 1$. Displacements have been magnified by a factor of 50.

The experimentally observed crack path of the four point SEN beam is a crack that curves down from the notch toward the lower right support. In continuum damage approaches one apparently needs to account for the influence of shear strains in the equivalent strain definition to obtain this crack path (see, e.g., Peerlings et al., 1998), although Rodriguez-Ferran and Huerta (2000) showed that the necessity to do so may very well be an artifact due to discretization errors. For the physically better motivated case of local exponential softening, it appears that the cohesive surface approach already predicts the correct crack path if only a damage initiation and growth criterion solely based on normal cohesive separation is used. Since the tangential separation parameter α does not show a large influence on the global characteristics of the fracture simulation, no conclusions can be drawn here as to which local softening behaviour resembles best the local fracture processes in concrete. Besides this issue, the influence of the discretization cannot be ruled out. This will be dealt with in the next section.

4.3. Mesh dependence

The integration over the cohesive surface area in the virtual work expression (12) is not restricted to a single cohesive surface, as done by e.g., Needleman (1987, 1990) and Xu and Needleman (1993). Xu and Needleman (1994) were the first to use cohesive surfaces interspersed throughout the material, thus allowing cracks to nucleate and grow without additional assumptions or criteria other than the cohesive surface constitutive response. The issue of mesh dependence in the cohesive surface methodology has not received much attention yet.

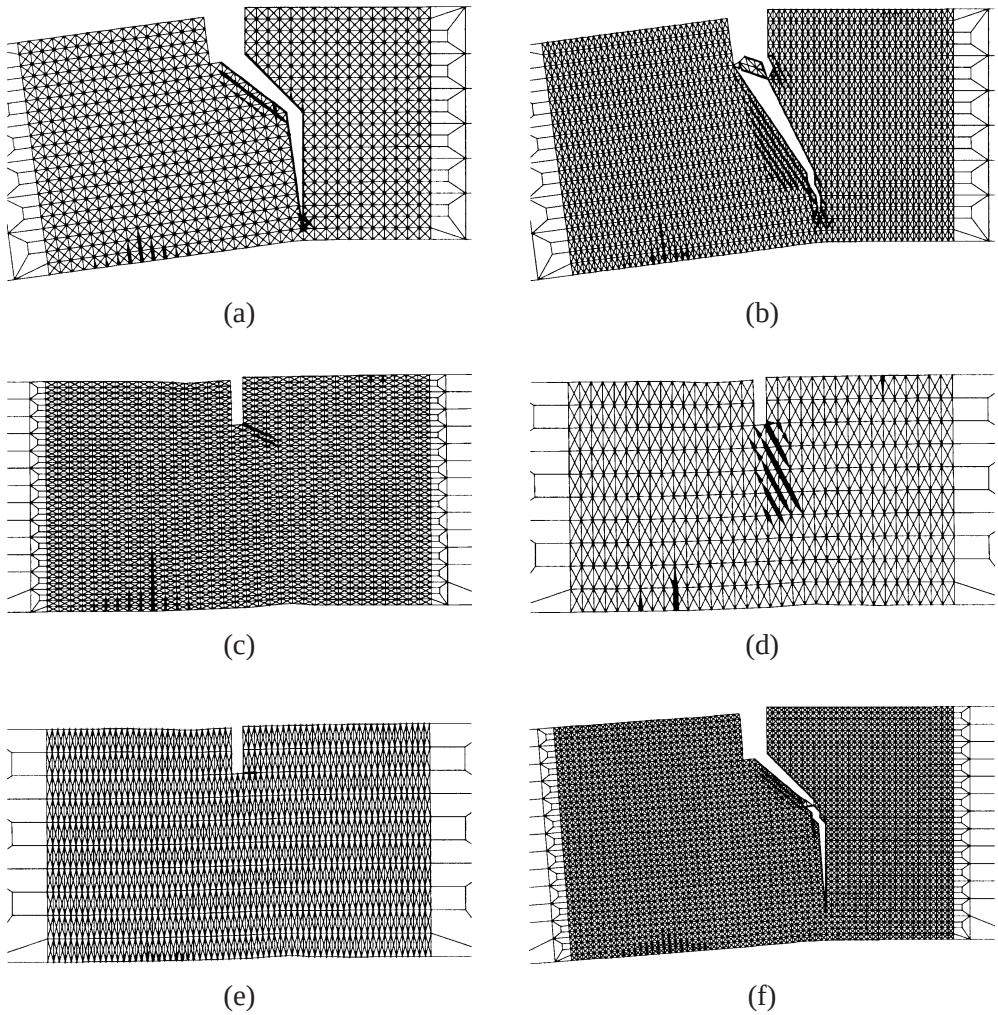

Figure 10. Influence of discretization using $\alpha = 0$, two-point Newton–Cotes integration and regular meshes. Dimensions of rectangular units: (a) 5×5 mm, (b) 2.5×5 mm, (c) 5×2.5 mm, (d) 5×10 mm, (e) 2.5×10 mm, (f) 2.5×2.5 mm.

In this section we will focus on three aspects of the numerical calculations related to mesh dependency. These are: (i) the influence of the numerical quadrature of the cohesive surface contribution, (ii) the influence of the tangential cohesive separation parameter α and (iii) the influence of mesh refinement. The calculations on the SEN beam have been performed with six different regular discretizations in a crossed triangle configuration. The rectangular elements have dimensions 5×5 mm, 2.5×5 mm, 5×2.5 mm, 5×10 mm, 2.5×10 mm and 2.5×2.5 mm. The final fracture path of the calculations are shown in *figure 10* for two-point Newton–Cotes integration and $\alpha = 0$, *figure 11* for two-point Gauss integration and $\alpha = 0$ and *figure 12* for two-point Newton–Cotes integration and $\alpha = 1$.

Schellekens and De Borst (1993) showed that spurious traction oscillations appear in the cohesive surfaces when the integration is carried out using Gauss quadrature. Although small traction oscillations also appear in the calculations of the SEN beam, it appears that Gauss quadrature yields slightly better curved crack paths. This is best seen when comparing *figure 10a* with *figure 11a* and *figure 10f* with *figure 11f*. The reason for this is that the traction oscillations only have an important influence if the gradients of traction are large. This

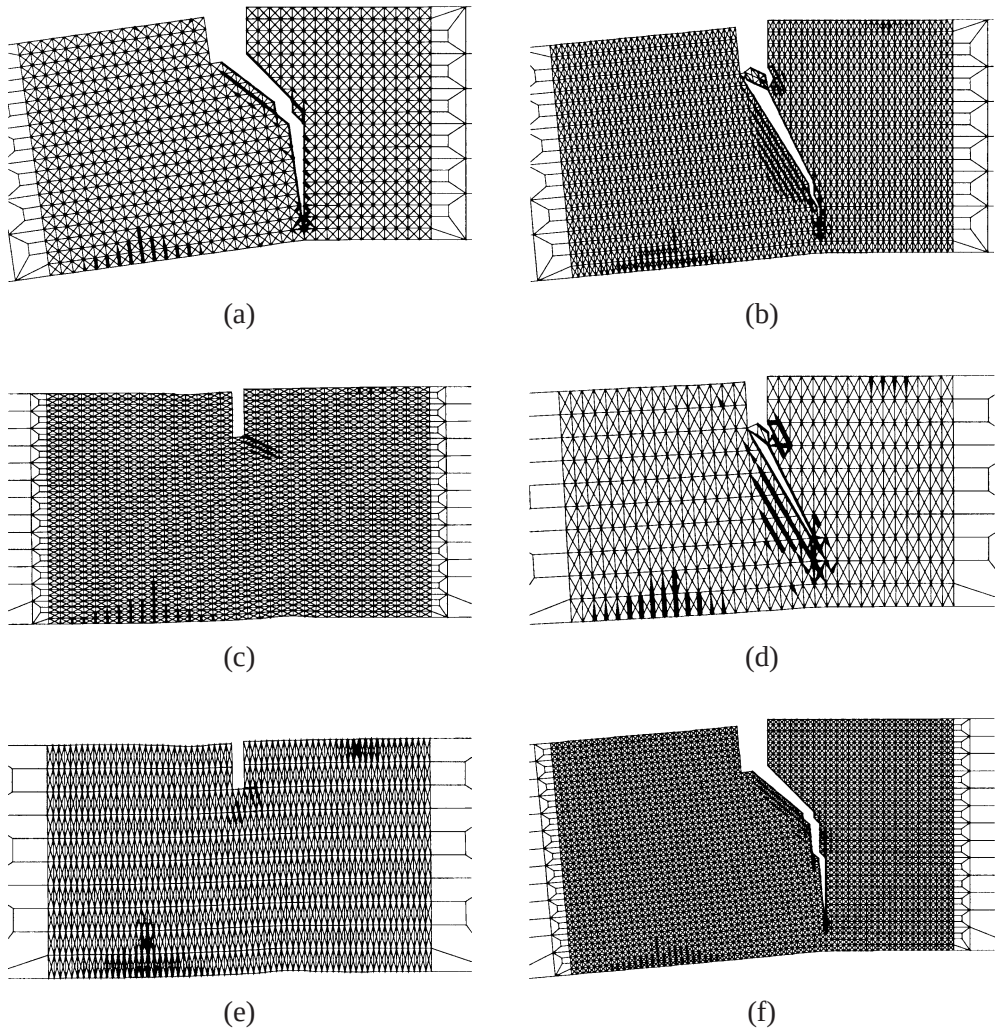

Figure 11. Influence of discretization using $\alpha = 0$, two-point Gauss integration and regular meshes. Dimensions of rectangular units in (a)–(f) as in *figure 10*.

is not the case in the present calculations because the discretization was taken fine enough to represent the smooth stress fields in this particular problem. Apart from the minor differences in crack path, the solution is not dominated by the type of quadrature. The load vs. CMSD curve shown in *figure 13* confirms this.

During the quasi-static calculations we often reach a point were the incremental solution jumps back and forth between two near-equilibrium states. The algorithm is not capable of passing such points. This situation becomes worse upon mesh refinement. When comparing the results in *figure 10* and *figure 11*, it is clear that the discretization has a strong influence on the failure pattern. For a regular 5×5 mm and 2.5×2.5 mm mesh we obtain good agreement with experimentally observed crack paths. However, with the non-square discretizations shown in *figures 10c–e* and *11c–e* an unsatisfactory solution is obtained.

Figures 12a–f show the resulting fracture paths for the SEN beam calculated with Newton–Cotes integration and $\alpha = 1$. Note that the unstructured meshes shown in *figure 8* and *figure 9* did not provide vertically oriented potential fracture paths, due to which the influence of the parameter α was not very pronounced. From the

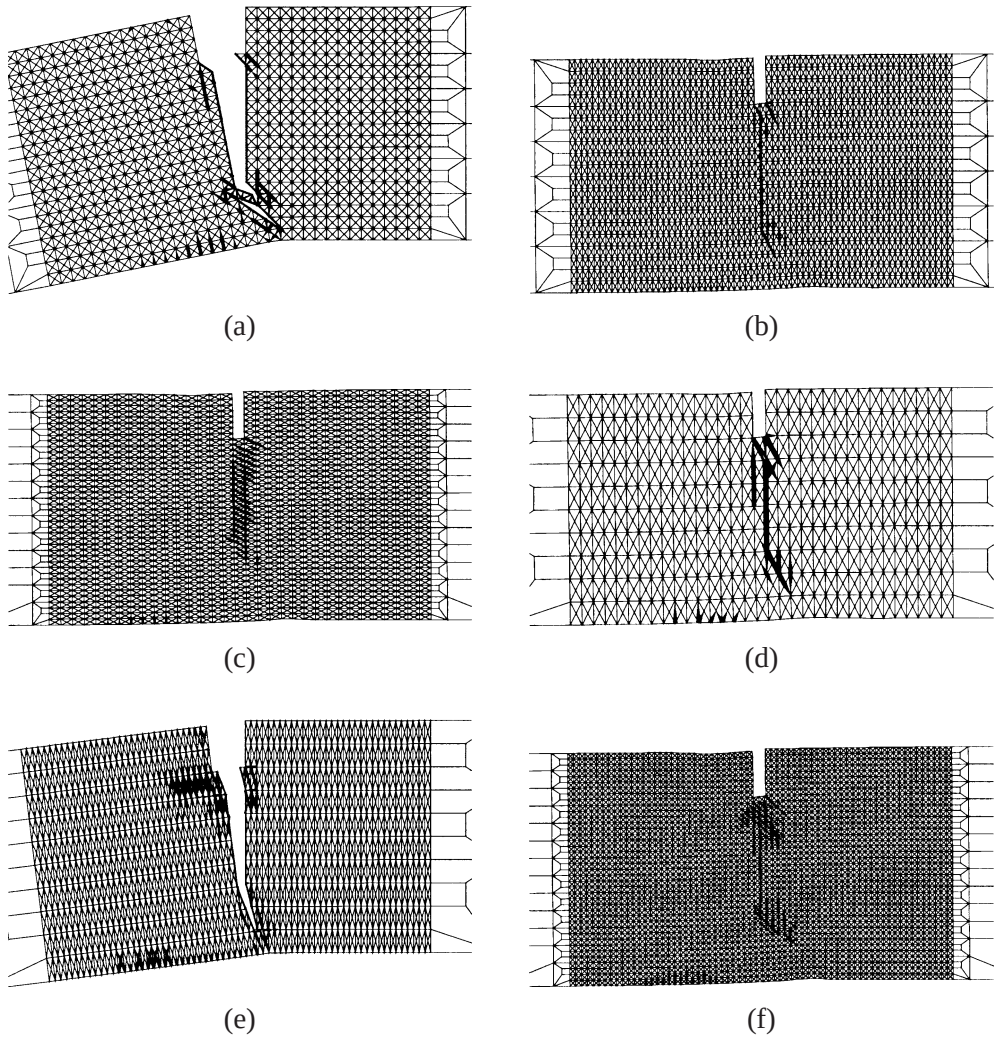

Figure 12. Influence of discretization using $\alpha = 1$, two-point Newton–Cotes integration and regular meshes. Dimensions of rectangular units in (a)–(f) as in *figure 10*.

calculations with the structured discretizations (*figure 12*) it is immediately clear that the influence of the tangential separation parameter α cannot be neglected now that a potential vertical crack path exists.

5. Application 2: Tensile test

5.1. Problem formulation

As a second application, the cohesive surface methodology will be applied to the fracture of a DEN specimen in tension. The geometry of the bar is taken equal to the specimens used in experiments conducted by Shi et al. (1999) and is depicted in *figure 14*. The specimens are 60 mm wide and 120 mm high. The thickness is 10 mm. The notches are 10 mm deep and 2 mm wide. The centreline of the notches have an offset of 0, 5, 10 or 15 mm. The experimental setup used by Shi et al. (1999) does not allow for rotation of the ends of the bar. In the

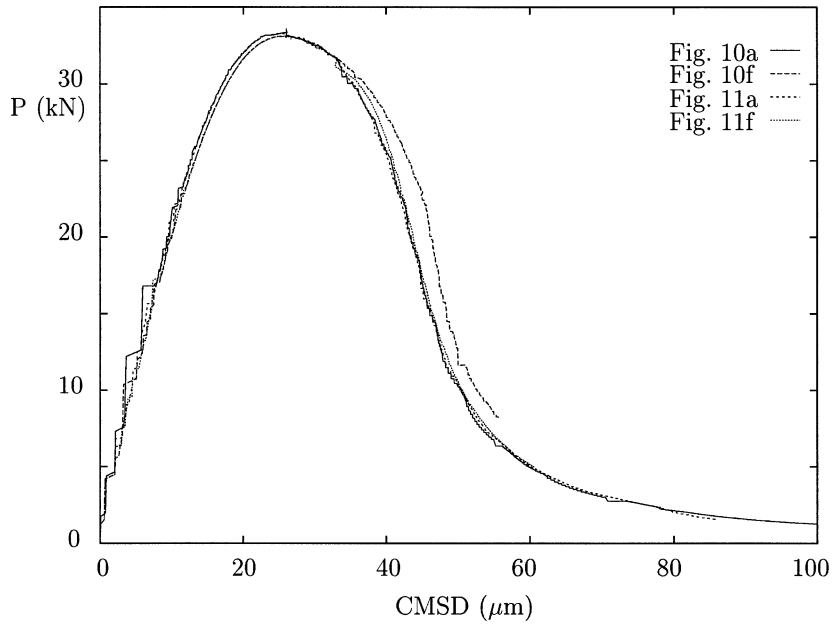

Figure 13. The influence of quadrature and mesh refinement on the load vs. crack mouth sliding displacement.

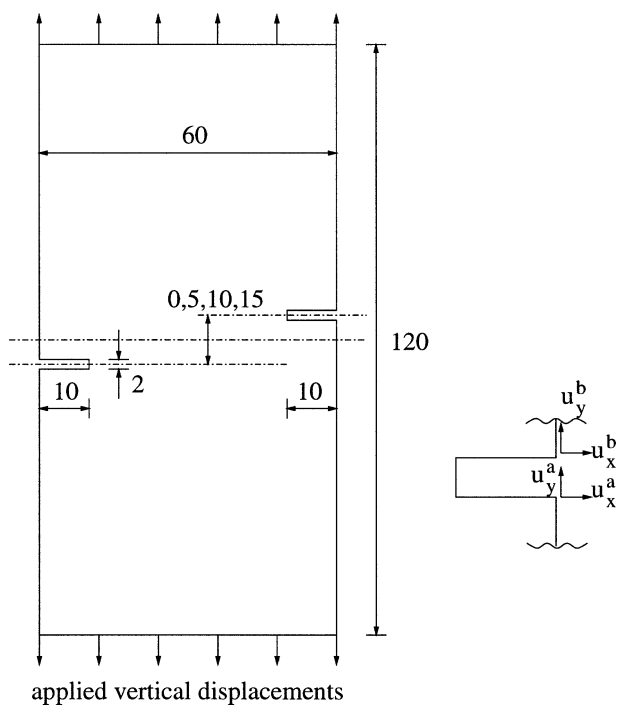

Figure 14. Configuration of the DEN-bar. All lengths are in mm.

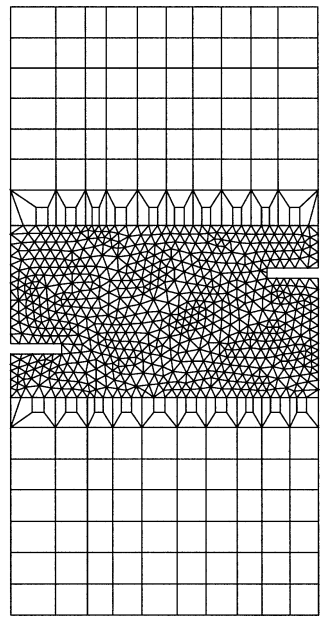

Figure 15. Finite element mesh of the DEN specimen.

numerical experiments a vertical displacement is prescribed at the top of the bar which is constant along the width. The applied displacement is prescribed by controlling the increase of the average crack mouth opening displacement of the notches, i.e. $\frac{1}{2}[(u_y^b - u_y^a)_{\text{left}} + (u_y^b - u_y^a)_{\text{right}}]$ in *figure 14*.

Fracture of the DEN tensile bar occurs in the centre section of the bar. To reduce computational effort cohesive surfaces are therefore only used in this centre section. A typical discretization of the beam is shown in *figure 15*. The material and cohesive surface parameters used in the calculations are identical to the values used for the SEN beam in the previous section. Based on the observations made in the previous section, we let the damage in the cohesive surface develop only due to the normal separation of the cohesive surface, i.e. $\alpha = 0$ in (4). The numerical integration of the cohesive surfaces is performed with two-point Gauss integration.

5.2. Results

Experiments (Shi et al., 1999) show that the cracks growing from both notches do not have a clear tendency to avoid or attract each other. Some experiments show that one of the cracks may get arrested while the other crack keeps growing and may or may not intersect with the arrested crack. Other experiments even show cracks growing away from each other.

Figures 16–19 show the calculated fracture paths obtained for all offsets. Each figure shows the result for one regularly discretized cohesive surface region and two different randomly discretized regions. The random discretizations show what is also observed in experiments. The cracks that grow from the notches sometimes do (*figure 16b* and *figure 17a*) and sometimes do not (*figure 16a* and *figure 18a*) grow towards each other.

The regular meshes clearly show that upon loading, the cracks tend to grow horizontally without much interaction. As the crack tips pass the centre of the bar, a damage zone in between the cracks forms. This does not affect the further growth of the crack. Only after further growth of the cracks the ligament in between the cracks is deformed in bending and judging from the damage zone at the crack tips, the cracks tend to deviate from their horizontal plane toward the notches. Since there is no restriction for the crack path to develop, it

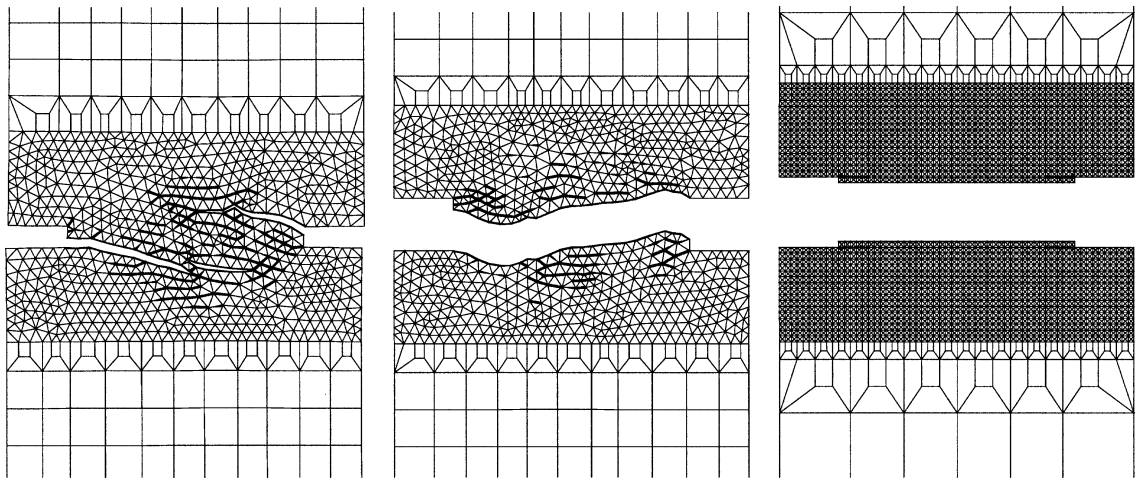

Figure 16. Influence of discretization on the predicted crack path for $d = 0$ mm. Displacements magnified by a factor of 50.

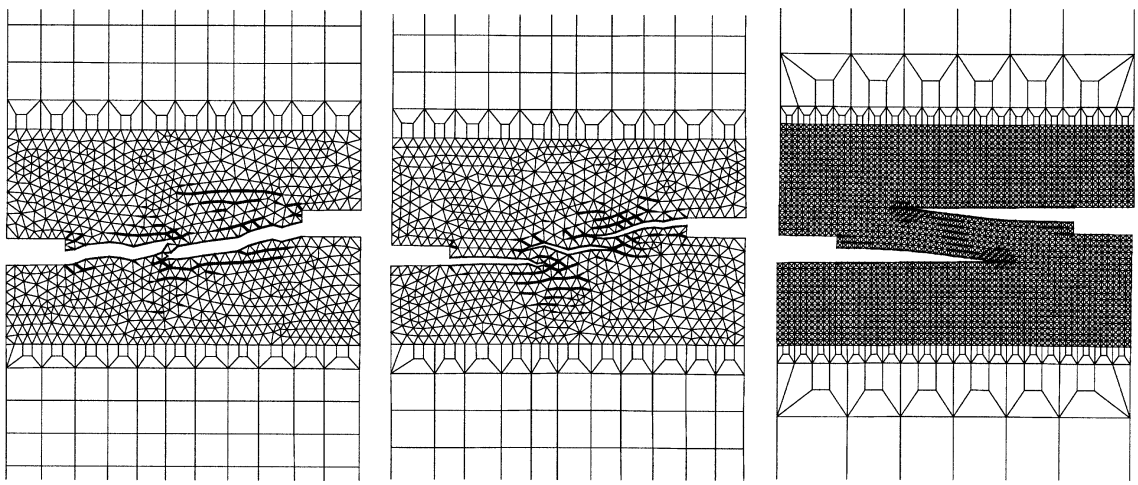

Figure 17. Influence of discretization on the predicted crack path for $d = 5$ mm. Displacements magnified by a factor of 50.

seems that in experiments the stress field is not responsible for the deviation of the crack from its horizontal path.

Plotting the global force, obtained as $P = \int_S \boldsymbol{\sigma} \cdot \boldsymbol{n}\, \mathrm{d}S$ at the top face of the DEN-bar, versus the CMOD, shown in *figure 20*, we see that the peak load is not much affected by the precise choice of the fracture path. The global peak load is always around 1.2 kN. This agrees with experimental results (Shi et al., 1999).

6. Concluding remarks

A cohesive surface constitutive model based on isotropic damage is presented. The model describes the development of cohesive tractions as a function of the normal and tangential separation. Coupling between these

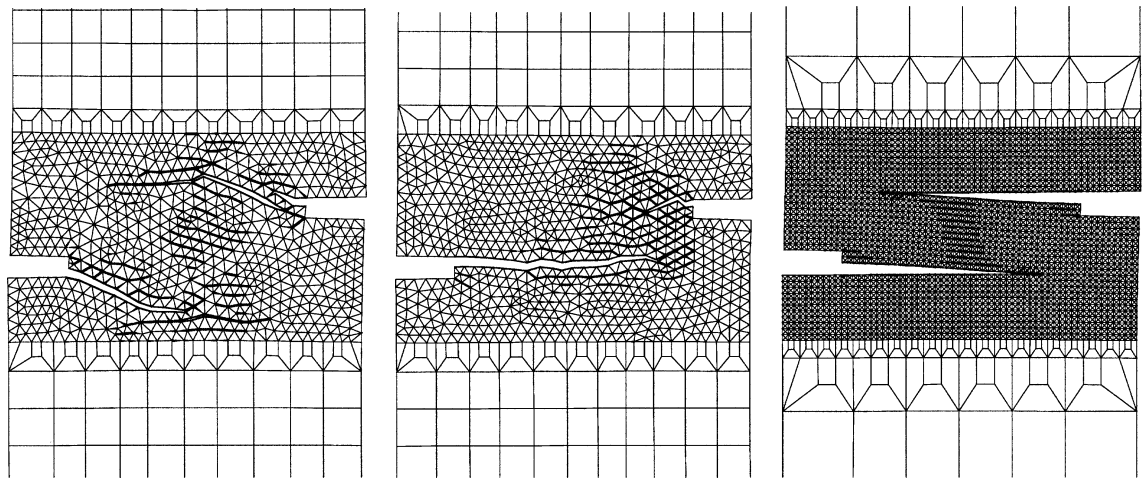

Figure 18. Influence of discretization on the predicted crack path for $d = 10$ mm. Displacements magnified by a factor of 50.

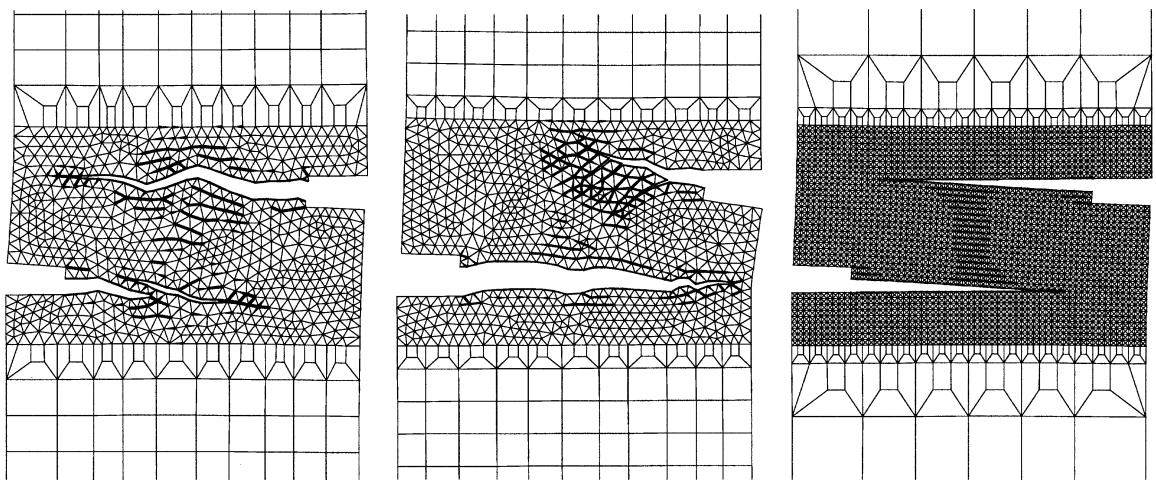

Figure 19. Influence of discretization on the predicted crack path for $d = 15$ mm. Displacements magnified by a factor of 50.

modes is obtained through the definition of an effective separation based on a weighted sum of the squares of the normal and tangential separation. The model is suitable for the calculation of fracture of concrete specimens at a macroscopic level, i.e. without accounting for the presence of aggregates.

The cohesive surface model is used for the single edge notched (SEN) four point shear beam and the double edge notched (DEN) direct tensile specimen. The results for the SEN beam show that local linear softening results in a global softening behaviour that is too brittle. Exponential softening gives a better response, but still the post-peak response is somewhat too brittle. The coupling between normal and tangential cohesive surface separation in the initiation and growth of damage in the presented formulation does not dominate the outcome of the solution. The simulations for the DEN specimen show good agreement with experimental observations, both with respect to local and global characteristics of the fracture process.

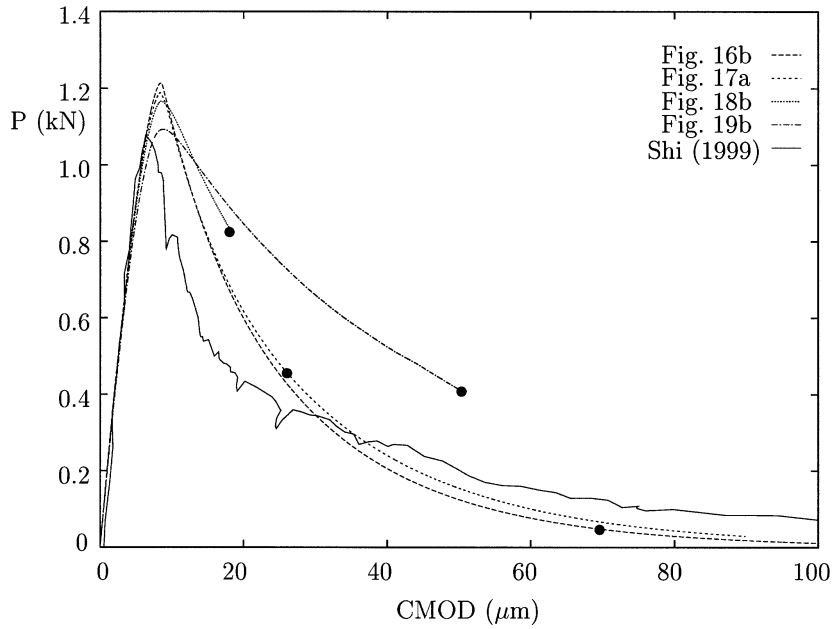

Figure 20. Representative force–CMOD curves for the DEN-bar. The dots indicate at which instants the snapshots in *figures 16–19* were taken.

The numerical results clearly show that the cohesive surface methodology exhibits a strong mesh alignment sensitivity. Since the cohesive surfaces represent potential fracture surfaces, the discretization with cohesive surfaces can be seen as an imprint of the microstructure of the underlying continuum. For the cohesive surface model used in this paper, which is suitable for the simulation of fracture of quasi-brittle materials, realistic fracture paths are therefore obtained only if the discretization resembles such a microstructure, i.e. the discretization must resemble a disordered structure. Despite the sensitivity of the fracture paths to the discretization, the global characteristics of the loading process, such as peak load, are not very sensitive to the discretization and are predicted with reasonable accuracy.

The mesh alignment sensitivity of the cohesive surface methodology as employed in this paper is a result of the restricted crack growth along continuum element boundaries. Recently, other methods to describe crack growth have appeared in the literature. The method of embedded discontinuities presented by Simo et al. (1993) uses enhanced assumed strains to allow for cracks to grow arbitrarily through continuum elements. A drawback of this method is that crack growth is not continuous over element boundaries. A solution to this problem was given by Oliver (1996). However, the robustness of this methodology is still an issue of concern. Belytschko and Black (1999) presented a method in which discontinuous enrichment functions are added to the finite element approximation. These enrichment functions account for the presence of a crack and crack growth is continuous over element boundaries. The enrichment functions used by Belytschko and Black (1999) were taken from the linear elastic fracture mechanics (LEFM) solution for the near-tip displacement fields for combined mode I and mode II loading. This restricts the method to applications in which LEFM is a valid approximation. It is conceivable that these restrictions can be lifted by combining the cohesive surface methodology with the approach presented by Belytschko and Black (1999).

References

de Borst R., Computation of post-bifurcation and post-failure behaviour of strain-softening solids, Computers and Structures 25 (1987) 211–224.

Bažant Z.P., Belytschko T., Chang T.-P., Continuum theory for strain-softening, J. Engg. Mech. 110 (1984) 1666–1692.

Bažant Z.P., Pijaudier-Cabot G., Nonlocal continuum damage, localization instability and convergence, J. Appl. Mech. 55 (1988) 287–293.

Belytschko T., Black T., Elastic crack growth in finite elements with minimal remeshing, Internat. J. Numer. Methods in Engg. 45 (1999) 601–620.

Camacho G.T., Ortiz M., Computational modelling of impact damage in brittle materials, Internat. J. Solids and Structures 33 (1996) 2899–2938.

Carol I., Prat P.C., López C.M., Normal/shear cracking model: Application to discrete crack analysis, J. Engg. Mech. 123 (1997) 765–773.

Fabrikant V.I., Complete solutions to some mixed boundary value problems in elasticity, Advances in Appl. Mech. 27 (1990) 153–223.

Fichant S., La Borderie C., Pijaudier-Cabot G., Isotropic and anisotropic descriptions of damage in concrete structures, Mechanics of Cohesive-Frictional Materials 4 (1999) 339–359.

Govindjee S., Kay G.J., Simo J.C., Anisotropic modelling and numerical simulation of brittle damage in concrete, Internat. J. Numer. Methods in Engg. 38 (1995) 3611–3633.

Hillerborg A., Modeer M., Petersson P.E., Analysis of crack formation and crack growth in concrete by means of fracture mechanics and finite elements, Cement and Concrete Research 6 (1976) 773–781.

Huang X., Karihaloo B.L., Tension softening of quasi-brittle materials modelled by single and doubly periodic arrays of coplanar penny-shaped cracks, Mechanics of Materials 13 (1992) 257–275.

Kachanov L.M., Introduction to Continuum Damage Mechanics, Nijhoff, Dordrecht, The Netherlands, 1986.

Kachanov M., Laures J.-P., Three-dimensional problems of strongly interacting arbitrarily located penny-shaped cracks, Internat. J. of Fracture 41 (1989) 289–313.

Koiter W.T., An infinite row of collinear cracks in an infinite elastic sheet, Ingenieur Archiv 28 (1959) 168–172.

Lourenço P.B., Rots J.G., Multisurface interface model for analysis of masonry structures, J. Engg. Mech. 123 (1997) 660–668.

Mazars J., Pijaudier-Cabot G., Continuum damage theory – application to concrete, J. Engg. Mech. 115 (1989) 345–365.

Meschke G., Lackner R., Mang H.A., An anisotropic elastoplastic-damage model for plain concrete, Internat. J. Numer. Methods in Engg. 42 (1998) 703–727.

Needleman A., A continuum model for void nucleation by inclusion debonding, J. Appl. Mech. 54 (1987) 525–531.

Needleman A., An analysis of decohesion along an imperfect interface, Internat. J. of Fracture 42 (1990) 21–40.

Oliver J., Modelling strong discontinuities in solid mechanics via strain softening constitutive equations. Part 2: Numerical simulation, Internat. J. Numer. Methods in Engg. 39 (1996) 3601–3623.

Ortiz M., Microcrack coalescence and macroscopic crack growth initiation in brittle solids, Internat. J. Solids and Structures 24 (1988) 231–250.

Peerlings R.H.J., de Borst R., Brekelmans W.A.M., Geers M.G.D., Gradient-enhanced damage modelling of concrete fracture, Mechanics of Cohesive-Frictional Materials 3 (1998) 323–342.

Peerlings R.H.J., de Borst R., Brekelmans W.A.M., de Vree J.H.P., Gradient-enhanced damage for quasi-brittle materials, Internat. J. Numer. Methods in Engg. 39 (1996) 3391–3403.

Pijaudier-Cabot G., Bažant Z.P., Nonlocal damage theory, J. Engg. Mech. 113 (1987) 1512–1533.

Rodriguez-Ferran A., Huerta A., Error estimation and adaptivity for nonlocal damage models, submitted to Internat. J. Solids and Structures (2000).

Schellekens J.C.J., De Borst R., On the numerical integration of interface elements, Internat. J. Numer. Methods in Engg. 36 (1993) 43–66.

Schlangen E., Experimental and numerical analysis of fracture processes in concrete, Heron 38 (2) (1993).

Shi C., van Dam A.G., van Mier J.G.M., Sluys L.J., Crack interaction in concrete, presented at EUROMAT 99, Munich, Germany, 1999.

Simo J.C., Oliver J., Armero F., An analysis of strong discontinuities induced by strain-softening in rate-independent inelastic solids, Computational Mechanics 12 (1993) 277–296.

Van Mier J.G.M., Fracture Processes of Concrete, CRC Press, New York, 1997.

Westmann R.A., Asymmetric mixed boundary-value problems of the elastic half-space, J. Appl. Mech. 32 (1965) 411–417.

Xu X.-P., Needleman A., Void nucleation by inclusion debonding in a crystal matrix, Modelling and Simulation in Materials Science and Engineering 1 (1993) 111–132.

Xu X.-P., Needleman A., Numerical simulations of fast crack growth in brittle solids, J. Mech. and Phys. of Solids 42 (1994) 1397–1434.